https://doi.org/10.5194/essd-2021-310
Preprint. Discussion started: 4 November 2021

Open Access Earth System Science Data Discussions

Observations of the Lower Atmosphere From the 2021 WiscoDISCO Campaign

Patricia A. Cleary[1], Gijs de Boer[2,3,4], Joseph P. Hupy[5], Steven Borenstein[4], Jonathan Hamilton[2,3], Ben Kies[1], Dale Lawrence[6], R. Bradley Pierce[7], Joe Tirado[1], Aidan Voon[1], Timothy Wagner[7]

[1] Department of Chemistry, University of Wisconsin Eau-Claire, Eau-Claire, WI, 54701, USA
[2] Cooperative Institute for Research in Environmental Sciences, University of Colorado Boulder, Boulder, CO, 80309, USA
[3] Physical Sciences Laboratory, National Oceanic and Atmospheric Administration, Boulder, CO, 80305, USA
[4] Integrated Remote and In Situ Sensing, University of Colorado Boulder, Boulder, CO, 80309, USA
[5] School of Aviation and Transportation Technology, Purdue University, West Lafayette, IN, 47907, USA
[6] Research and Engineering Center for Unmanned Vehicles, University of Colorado Boulder, Boulder, CO, 80309, USA
[7] Space Science and Engineering Center, University of Wisconsin Madison, Madison, WI, 53706, USA

Correspondence to: Patricia A. Cleary (clearypa@uwec.edu)

Abstract. The meso-scale meteorology of lake breezes along Lake Michigan impacts local observations of high ozone events. Previous manned aircraft and UAS observations have demonstrated non-uniform ozone concentrations within and above the marine layer over water and within shoreline environments. During the 2021 Wisconsin's Dynamic Influence of Shoreline Circulations on Ozone (WiscoDISCO-21) campaign, two UAS platforms, a fixed-wing (University of Colorado RAAVEN) and a multirotor (Purdue University DJI M210), were used simultaneously to capture lake breeze during forecasted high ozone events at Chiwaukee Prairie State Natural Area in southeastern Wisconsin from May 21-26, 2021. The RAAVEN platform (data DOI: 10.5281/zenodo.5142491) measured temperature, humidity, and 3-D winds during 2-hour flights following two separate flight patterns up to 3 times per day at altitudes reaching 500 m above ground level. The M210 platform (data DOI: 10.5281/zenodo.5160346) measured vertical profiles of temperature, humidity and ozone during 15-minute flights up to 6 times per day at altitudes reaching 120 m above ground level (AGL) near to a WI-DNR ground monitoring station (AIRS ID: 55-059-0019). This campaign was conducted in conjunction with the Enhanced Ozone Monitoring plan from WI-DNR that included Doppler lidar wind profiler observations at the site (data DOI:10.5281/zenodo.5213039).

https://doi.org/10.5194/essd-2021-310
Preprint. Discussion started: 4 November 2021

Open Access Earth System Science Data Discussions

1. Introduction

The WiscoDISCO-21 (Wisconsin's Dynamic Influence on Shoreline Circulations on Ozone) was designed to capture lake breeze influence on shoreline ozone observations and to interrogate the low-altitude dimensionality of the marine layer as it moves on shore. The influence of lake breeze on shoreline air quality along Lake Michigan (Keen and Lyons, 1978; Lyons and Cole, 1976; Lyons and Olsson, 1973; Dye et al., 1995; Foley et al., 2011; Stanier et al., 2021) and other Great Lakes (Hayden et al., 2011; Levy et al., 2010; Wentworth et al., 2015; Sills et al., 2011) is well documented by campaigns incorporating ground (Lyons and Cole, 1976), ferry (Lennartson and Schwartz, 2002; Cleary et al., 2015) and aircraft observations (Dye et al., 1995; Foley et al., 2011; Hayden et al., 2011; Stanier et al., 2021). The shoreline communities of Lake Michigan have historically been in non-attainment of federal ozone standards. Precursors to ozone production have emission sources along the Chicago urban corridor and ozone production can be enhanced when those emissions are trapped in the marine layer over the lake and get transported northward from Chicago (Vermeuel et al., 2019; Dye et al., 1995; Foley et al., 2011). The low altitude features in ozone gradients over Lake Michigan have been observed in the recent 2017 Lake Michigan Ozone Study field campaign (Stanier et al., 2021; Doak et al., 2021). Stanier, et al. (2021) describe observations for the highest measured ozone during the field campaign existing over water, offshore from Milwaukee and in the altitude range of 30-100 m above lake level. The shallow marine layer disruption when crossing a shoreline boundary during a lake breeze is a unique environment to study the changes in vertical mixing and pollutant extent.

WiscoDISCO-21featured round-based Doppler lidar observations and two Uncrewed Aircraft Systems (UAS), including the University of Colorado RAAVEN fixed-wing UAS and Purdue University's DJI M210 quadcopter. These platforms were deployed to enhance the level of detail and extend the domains of ground-based measurements to manned aircraft observations with higher spatial resolution and sustained lower-altitude flight. UAS are well suited to make observations of a shoreline environment impacted by a shallow marine layer, where vertical mixing and pollutant transport are key to understanding pollution events at the surface. UAS have been used in riverine environments to highlight pollutant transport and night time boundary layer dynamics (Guimaras et al., 2020). During the Ozone

https://doi.org/10.5194/essd-2021-310
Preprint. Discussion started: 4 November 2021


Open Access Earth System Science Data Discussions

Water-Land Environmental Transition Study (OWLETs), UAS, ozone sondes and lidar observations were used to observe ozone titration events above the Chesapeake Bay shipping channel (Gronoff et al., 2019). Horel et al., (Horel et al., 2016) describe the use of distributed ground sensors, tethered sondes and UAS to better understand the meteorological and pollutant transport factors surrounding poor air quality in the Salt Lake Valley. Incorporation of multi-hole probes into fixed-wing UAS has allowed for observations of 3-D winds (Elston et al., 2015) and turbulent fluxes (Wildmann et al., 2014). The RAAVEN platform leveraged in WiscoDISCO-21 has recently been used to study the lower atmosphere across a variety of environmental regimes. This includes nearly a month of flight operations to investigate the thermodynamic and kinematic structure of trade winds over the tropical Atlantic Ocean, (de Boer et al. 2021a) as well as deployments to the US Midwest to make measurements of supercell thunderstorms (Frew et al., 2020). The measurement accuracy of the RAAVEN's instrumentation was recently evaluated at the US Department of Energy's Atmospheric Radiation Measurement (ARM) program's Southern Great Plains facility (see de Boer et al. (2021b) for details).

Such high-resolution UAS observations are well-suited for documenting and characterizing the dimensions of the lake breeze phenomenon and corresponding pollutant transport. A combination of UAS and lidar can provide overlapping domains of observations that scale up to planetary boundary layer heights, with UAS providing detailed insight into nonuniformities in meteorological observations along the Lake Michigan shoreline. UAS observations are particularly complementary to Doppler lidar observations, as such observations are subject to near-field issues that prevent them from making observations at very low altitudes. Given that the UAS readily operate between the surface and 100 m, these platforms can fill in this gap and provide detailed insight into thermodynamic, kinematic and chemical properties of this layer. These observations have higher vertical and temporal resolution than many chemical models which can provide insight into model resolution issues at the lake-land interface (Wagner et al., 2021). The WiscoDISCO-21 field campaign was conducted in conjunction with the Enhanced Ozone Monitoring initiative from the Wi-DNR who housed added instrumentation for NO, NO_y, NO_x, VOC canisters and PANDORA instrumentation at the Chiwaukee Prairie air monitoring

https://doi.org/10.5194/essd-2021-310
Preprint. Discussion started: 4 November 2021


Open Access Earth System Science Data Discussions

station. The WiDNR has provided a portal for access to data from these sensors through their web portal (https://wi-dnr.widencollective.com/portals/iwvftorq/AirMonitoringData).

2. Description of measurement location, deployment strategies and sampling

The Chiwaukee Prairie State Natural Area is a 485-acre shoreline prairie managed by the Wisconsin Department of Natural Resources (WiDNR) located along the shoreline of Lake Michigan and adjacent to the Wisconsin/Illinois border. The WiDNR operates an air monitoring station (Airs ID 55-059-0019) for Kenosha County within this area, located at 11838 First Court in Pleasant Prairie, WI. This location was chosen due to its suitability for UAS flight operations and the regular influence of lake breeze circulations at the site. As a result of these lake breezes, the WiDNR's Chiwaukee Prairie Monitor regularly observes some of the highest ozone concentrations in the state (Stanier et al., 2021). Land use in the region is mixed suburban housing and farming, with two marinas directly south of the research site. Chiwaukee Prairie has trail access along Al Kemper Trail and 122nd Street that is isolated from automobile, bicycle and most pedestrian traffic. The M210 flights were conducted near to the WiDNR Air Monitoring site (Latitude: 42.5045, Longitude: -87.8095) and the RAAVEN flight operations were conducted on Al Kemper Trail or 122nd St to provide ample room for take-off and landing (Fig. 1).

https://doi.org/10.5194/essd-2021-310
Preprint. Discussion started: 4 November 2021

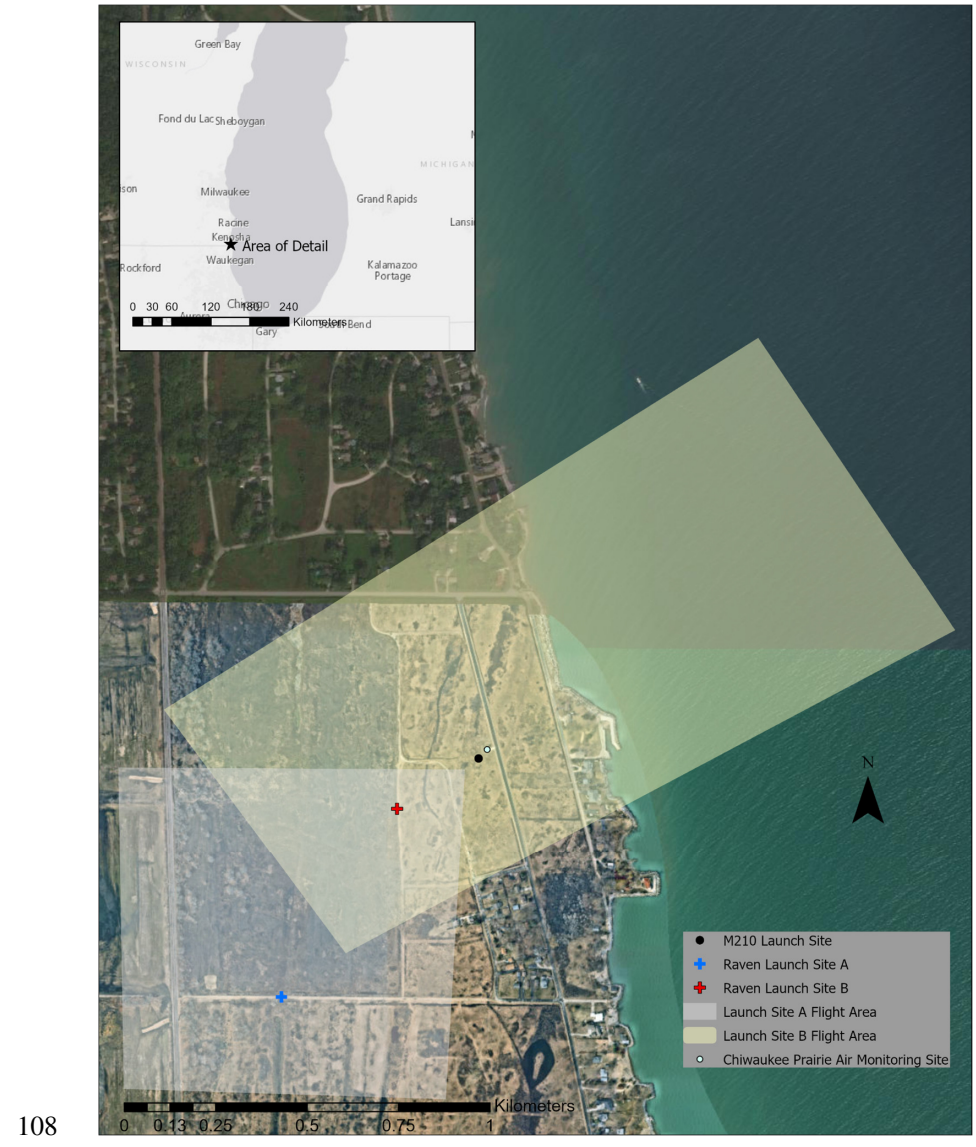

Figure 1: Research site map including Chiwaukee Prairie air monitor and locations for launch sites for M210 and RAAVEN. Map created using Esri ArcPro version 2.52 using ArcPro basemap imagery.

https://doi.org/10.5194/essd-2021-310
Preprint. Discussion started: 4 November 2021

The primary goal for the field campaign was to capture elevated ozone concentration events resulting from lake breeze circulations at the site. The deployment strategy for selecting a time window for field operations was dictated by ozone and meteorological forecasts that predicted light southerly winds for an extended period that would both a) increase the likelihood of onshore lake breeze flow from weaker southerly winds and b) drive pollutant transport from the Chicago metro area to the site. Forecasts from both the WiDNR and Realtime Air Quality Modeling System (RAQMS) were used to select an ideal deployment period. The dates of May 21-26, 2021 were chosen as meeting those requirements. Flights were cancelled during days in which high ozone or southerly/southeasterly lake breeze were not expected (Table 1).

Table 1: UAS flight days and conditions for the WiscoDISCO-21 field campaign

Date (2021)	M210 (time UTC)	University of Colorado RAAVEN (Time UTC and flight pattern)	Weather and Air Quality Conditions
Friday, May 21	F1 (15:35-15:44) F2 (16:38-16:47) F3 (19:08-19:21) F4 (19:46-19:59)	F1 (15:01-16:54) Pattern A F2 (18:36-20:40) Pattern A	SW wind, Temps > 25 ^{o}C, small shift in winds to colder from SSE
Saturday, May 22	F1 (14:22-14:35) F2 (15:18-15:31) F3 (17:27-17:41) F4 (18:26-18:41) F5 (20:09-20:22) F6 (20:59-21:14)	F1 (13:52-15:55) Pattern A F2 (17:00-19:03) Pattern A F3 (19:30-21:38) Pattern A	W wind in AM, Temps > 25 ^{o}C, consistent shift in winds to colder from SSE.
Sunday, May 23	no flights	no flights	W to NE winds, dropping temperatures, AM showers, PM showers
Monday, May 24	F1 (15:08-15:23) F2 (16:01-16:16) F3 (18:14-18:29) F4 (19:12-19:27)	F1 (14:24-16:30) Pattern B F2 (17:41-19:50) Pattern B	S winds, lake breeze, high ozone event (> 70 ppb).

https://doi.org/10.5194/essd-2021-310
Preprint. Discussion started: 4 November 2021

	F5 (21:09-21:19) F6 (22:04-22:19)	F3 (20:42-22:51) Pattern B	
Tuesday, May 25	F1 (14:00-14:15) F2 (14:49-15:04)	F1 (13:39-15:42) Pattern B	SW winds, slight lake breeze in the morning, overtaken by westerlies
Wednesday, May 26	F1 (13:43-13:58) F2 (14:37-14:52) F3 (16:47-17:02) F4 (17:47-18:01) F5 (19:51-20:06) F6 (20:48-21:01)	F1 (13:27-15:24) Pattern B F2 (16:31-18:20) Pattern B F3 (19:30-21:22) Pattern B	W wind, steady all day, sunny. After all flights, lake breeze came in from NE

Flights were conducted in the time window 08:00-17:00 local time, CDT (13:00-22:00 UTC) (Table 1). The RAAVEN platform features 2-hour flight times and was deployed to complete up to 3 flights per day. The M210 flew slow ascents to 120 m AGL with an approximate 15-minute flight time, completing up to 6 flights per day and the sampling pattern was designated to achieve maximum overlap with the RAAVEN flight times by conducting two flights per RAAVEN flight.

During WiscoDISCO-21, the RAAVEN completed 12 flights, totaling 25.4 flight hours, operating under a Certificate of Authorization (COA) from the US Federal Aviation Administration (FAA) to allow flights up to 518 m AGL. Fig. 2a shows a map of the RAAVEN flights, while figure 2b includes a histogram of the altitudes covered by these flights. Flights were designed to follow two distinct flight patterns to capture over-prairie profiles using a circular pattern with holding at altitudes 400, 250, 150, 100 and 50 m AGL and over-water/over-prairie profiles using an extended racetrack pattern that traversed the shoreline, with holding altitudes at 400, 250, 150, 100 and 50 m AGL (see Figure 2c for the two flight patterns). Figure 3 shows histograms of the measurements obtained by the RAAVEN over the length of the campaign, including temperature, relative humidity, wind speed, wind direction, air pressure, and surface and sky brightness temperature.

https://doi.org/10.5194/essd-2021-310
Preprint. Discussion started: 4 November 2021

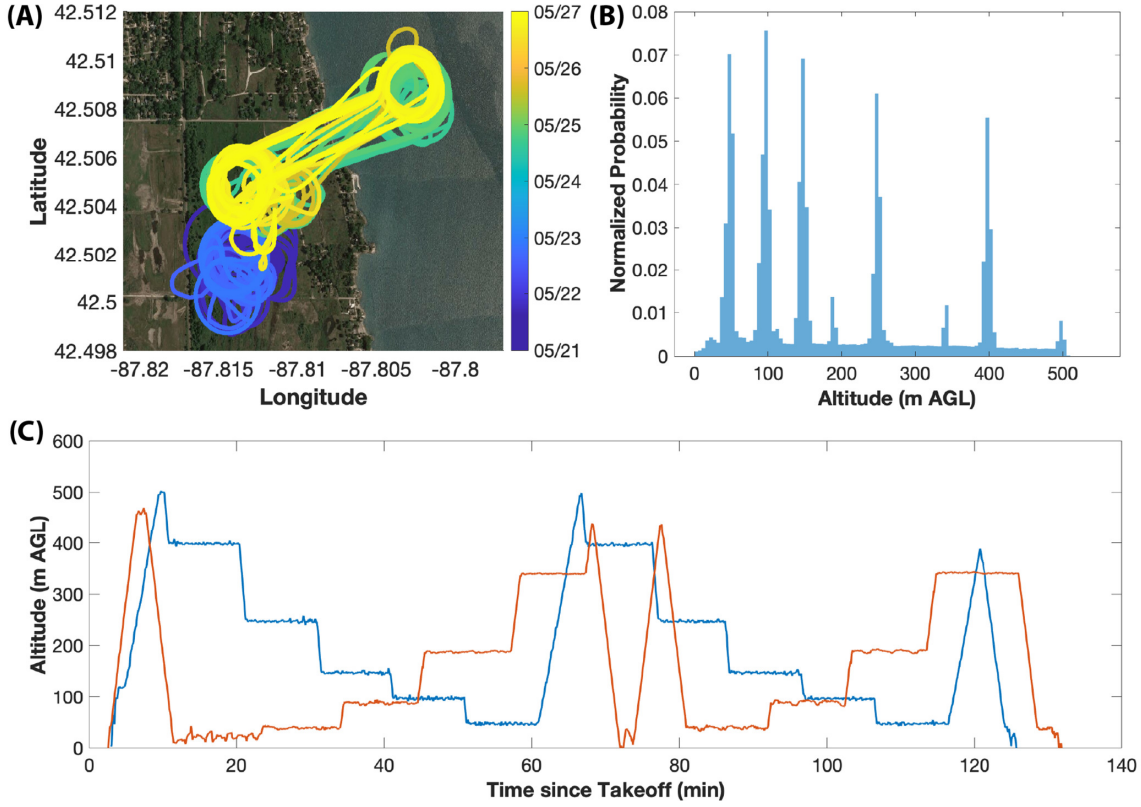

Figure 2: A map showing the flight tracks for the RAAVEN (a), a histogram of altitudes sampled by the RAAVEN (b), and example time-height plots of the two types of RAAVEN flights (c). Background maps are © GoogleMaps 2021, downloaded through their API.

https://doi.org/10.5194/essd-2021-310
Preprint. Discussion started: 4 November 2021

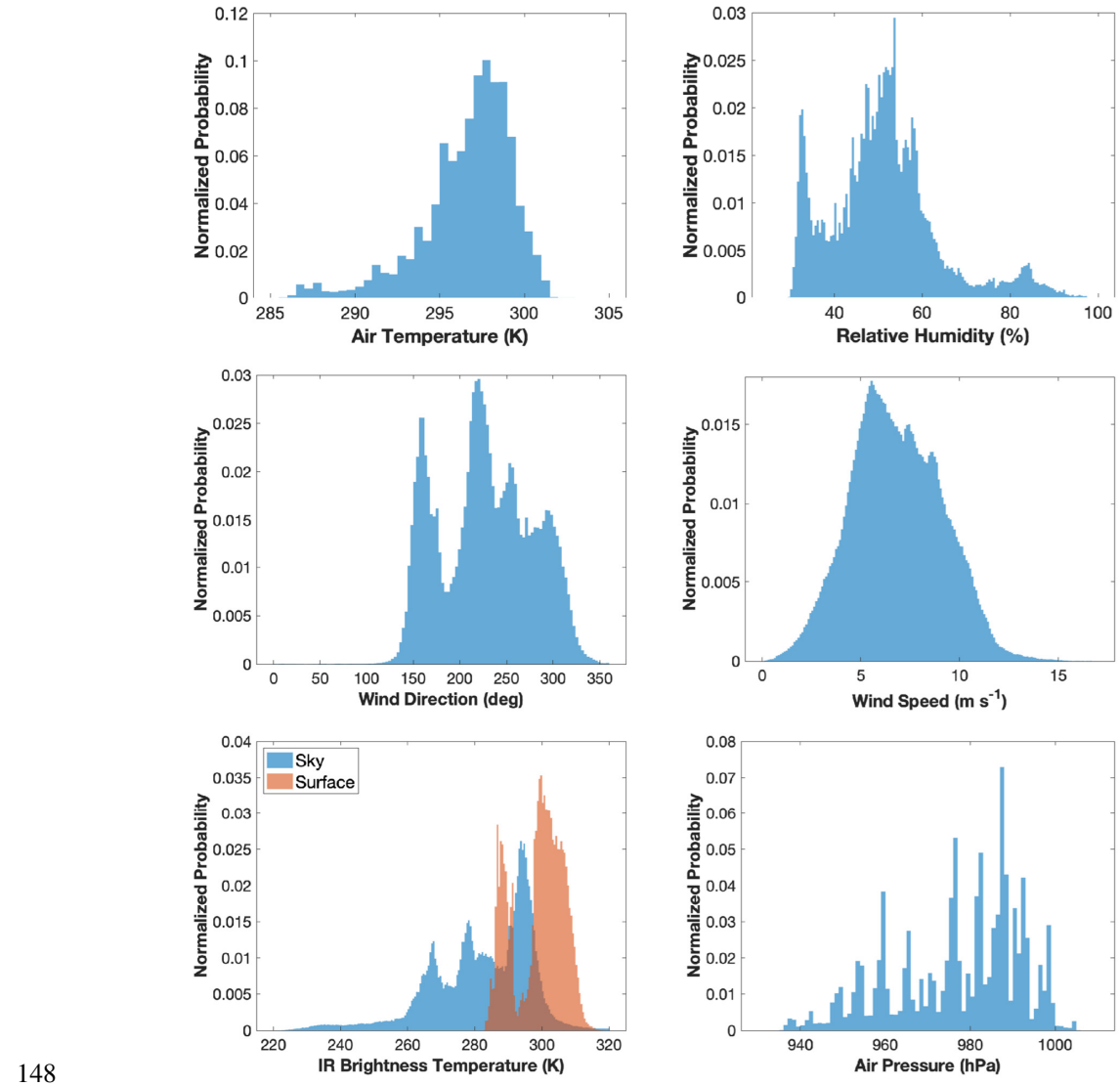

Figure 3: Histograms of (clockwise from top left) temperature, relative humidity, wind speed, pressure, IR brightness temperatures, and wind direction, as measured by the RAAVEN during WiscoDISCO-21.

https://doi.org/10.5194/essd-2021-310
Preprint. Discussion started: 4 November 2021

3. Description of Instrumentation and Vehicles

3.1 University of Colorado RAAVEN UAS

The RAAVEN UAS (Fig. 4) is a fixed-wing UAS with a wingspan of 2.3 m that has been operated by the University of Colorado Boulder since 2019. The RAAVEN's airframe is based on a custom-manufactured model from RiteWing RC. The airframe has been updated to meet the needs of atmospheric science missions spanning a variety of environments. The RAAVEN leverages the PixHawk2 autopilot system and employs an 8S 21000 mAh Lithium Ion (Li-Ion) battery pack to offer flight times around 2.5 hours, depending on conditions and executed flight patterns. Specific modifications to the airframe include the integration of a tail boom to enhance longitudinal stability and improve the platform's performance. The aircraft has a top airspeed of approximately 130 km hr , though operations during WiscoDISCO-21 were almost exclusively conducted in the 60-70 km hr^{-1} range.

https://doi.org/10.5194/essd-2021-310
Preprint. Discussion started: 4 November 2021

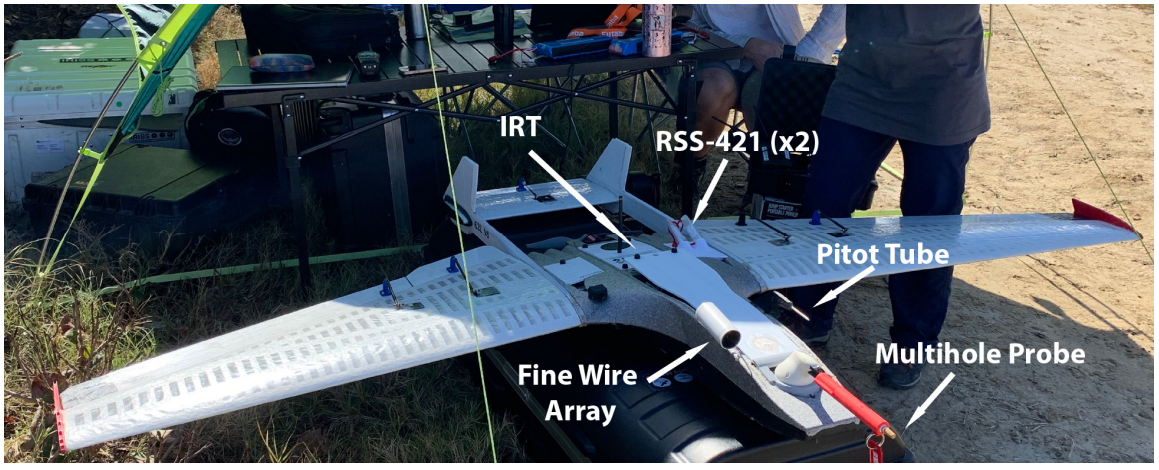

Figure 4: The University of Colorado RAAVEN being prepared for launch during WiscoDISCO21 (top), and a close up of the RAAVEN sensing systems (bottom).

For the WiscoDISCO-21 campaign, the RAAVEN was equipped with an instrument suite derived from the *miniFlux* payload co-developed by the National Oceanic and Atmospheric Administration (NOAA), the Cooperative Institute for Research in Environmental Sciences (CIRES) and Integrated Remote and In Situ Sensing (IRISS) at the University of Colorado. In this configuration, the aircraft was set up to measure atmospheric and surface properties to support evaluation of thermodynamic state, kinematic state, and turbulent fluxes of heat and momentum. This involves a suite of core instrumentation (see Fig. 3), including a multihole pressure probe (MHP) from Black Swift Technologies, LLC (BST), a pair of RSS421 PTH (pressure, temperature, humidity) sensors from Vaisala, Inc., a custom finewire array, developed and manufactured at the University of Colorado Boulder, a pair of Melexis MLX90614 IR thermometers, and a VectorNav VN-300 inertial navigation system (INS). This sensor suite is logged using a custom- designed FlexLogger data logging system.

The Vaisala RSS421 sensors are identical to those used in the Vaisala RD41 dropsonde, and very similar to the Vaisala RS41 radiosonde. This unit employs a linear resistive platinum temperature sensor with a resolution of 0.01 °C, repeatability of 0.1 °C and a response time (as measured within the RS41

https://doi.org/10.5194/essd-2021-310
Preprint. Discussion started: 4 November 2021


Open Access Earth System Science Data Discussions

radiosonde) of 0.5 s at 1000 hPa when moving at 6 m s^{-1}. For relative humidity (RH), the RSS421 includes a thin-film capacitor with a resolution of 0.1% RH and a repeatability of 2% RH, with a temperature-dependent response time of better than 0.3 s at 20 °C (again, as measured within the RS41, with 6 m s^{-1} airflow at 1000 hPa). Finally, the pressure sensor is capacitive with a silicon diaphragm, having a resolution of 0.01 hPa and a repeatability of 0.4 hPa. For WiscoDISCO-21, a pair of these sensor modules was mounted to the top of the RAAVEN's fuselage, between the nose and the tail of the aircraft on the port side. The sensor mounting angles were offset to ensure that the two sensors would have different amounts of solar exposure as the aircraft maneuvers through the atmosphere and to allow for the detection of solar heating effects since no shading is used. Additional information on atmospheric thermodynamic state is available from an E+E EE-03 sensor that is integrated into the BST MHP and from a Sensiron SHT-85 sensor that is integrated in the custom finewire array. The EE-03 has a temperature accuracy (at 20 °C) of 0.3 °C, while the humidity accuracy is stated to be 3% RH at 21 °C. The SHT-85 has a stated temperature accuracy of 0.1 °C (from 20-50 °C) and a repeatability of 0.08 C, while the humidity sensor has a stated accuracy of 1.5% RH and a repeatability of 0.15 % RH. Both the EE03 and the SHT-85 sensors have slower response times than the RSS421 sensor described above and are typically not used for scientific purposes unless there is a complete failure of the RSS421.

In addition to the SHT-85 sensor, the finewire array consists of two 5 μm diameter platinum wires extending over a 2 mm length, suspended in the free stream by supporting prongs. One wire is operated as a hotwire anemometer, with approximately 100 °C overheating compared to the ambient environmental temperature. The other wire is operated as a coldwire thermometer, with approximately 1 °C overheating relative to the surrounding environment. The wires have thermal time constants of 0.5 ms in a 15 m s^{-1} airflow regime and support a sampling frequency of up to 800Hz to support measurement of turbulent fluctuations in velocity and temperature. An electronics module converts resistance change in the wires due to velocity or temperature variability to amplified voltages. For WiscoDISCO-21, the finewire was logged at 250 Hz by the FlexLogger, which is equivalent to a 7.2 cm minimum length scale at the RAAVEN's typical cruise airspeed of 18 m s. Time series of these recorded data are processed during post-flight analysis to transform the voltages recorded by the fine wire module to velocity and

https://doi.org/10.5194/essd-2021-310
Preprint. Discussion started: 4 November 2021


Open Access Earth System Science Data Discussions

212 temperature. Additionally, these measured quantities can be fit to inertial sub-range turbulence models to
213 wavenumber spectra over suitable time intervals, producing turbulence intensity parameters epsilon
214 (kinetic energy dissipation rate) and CT^2 (temperature structure constant). The resolution (noise floor) of
215 these parameterizations is $2.0x10^{-7}$W kg^{-1} for epsilon and 4.5x10 K m for CT^2. Resolution of the raw time
216 series are 8.3x10 m s for the hotwire and 1.3x10 K for the coldwire.
217
218 In addition to the EE-03 PTH measurements, the BST 5-hole probe supports measurement of airspeed,
219 angle of attack (α) and sideslip angle (β). These measurements are combined with the GPS-based ground
220 velocities and aircraft attitude from the VectorNav VN-300 to derive the three-components of the inertial
221 wind (u, v, w), as discussed in section 4. The VN-300 can be configured in a dual-Global Navigation
222 Satellite System (GNSS) mode, under which the relative positions of two GNSS antennae are used to
223 calculate the platform yaw. However, this setting was not used during the WiscoDISCO-21 deployment.
224 Under dynamic conditions, the system has a stated accuracy of 0.3 degrees in GPS- Compass heading,
225 0.1 degrees in pitch and roll, 2.5 m horizontal position accuracy, 2.5 m vertical position accuracy when
226 integrating information from the barometric pressure sensor, and 0.05 m s^{-1} accuracy in inertial velocity.
227 Input from the system's gyroscope, accelerometer, GNSS receiver, magnetometer and pressure sensor are
228 filtered through an extended Kalman Filter (EKF) to produce a navigation solution. VN-300 data were
229 logged at 50 Hz resolution during WiscoDISCO-21.
230
231 Finally, RAAVEN deploys two Melexis MLX90614 IR thermometers: one looking up from the top of
232 the aircraft and one looking down towards the surface in level flight. These sensors are factory calibrated
233 to work in operational temperatures between -40 and 125 C, and to measure target brightness temperatures
234 between -70 and 380 °C. They have a high accuracy (0.5 °C) and a measurement resolution of 0.02 °C.
235 The RAAVEN-mounted MLX90614s are not stabilized to maintain a vertical orientation, meaning that
236 the observed target is perpendicular to the reference frame of the aircraft. This requires some care when
237 interpreting measurement from time periods when the aircraft is conducting pitch or rolling maneuvers.
238 For WiscoDISCO-21, we leveraged the "I" version of this sensor which has a 5-degree field of view.
239 These sensors have a broad passband range of 5-14 μm, meaning that while it covers the infrared

https://doi.org/10.5194/essd-2021-310
Preprint. Discussion started: 4 November 2021

atmospheric window, it is also subject to radiation emitted by water vapor and other radiatively active gases, meaning that a significant depth of atmosphere between the aircraft and a given target (e.g., cloud; surface), atmospheric gases influence the temperature reading. Despite this range spanning the 9.6 μm O_3 band, the relative proximity of the sensor to targets of interest (e.g. surface, clouds) means that this overlap is not expected to significantly influence the readings, due to the integrated path length being relatively small. Therefore, if absolute accuracy of brightness temperature is important, the sensor should be operated in close proximity to a target of interest. However, relative contributions from different surface types or atmospheric conditions can still be easily distinguished despite a lack of absolute calibration for extended distance sensing. Such gradient detection can be useful for detecting surface inhomogeneities, or for understanding whether the aircraft is operating under cloud or clear sky.

3.2 M210 UAS

The DJI M210 quad copter was equipped with a 3-D printed top-mounted bracket for holding a 2B Technologies Personal Ozone Monitor (POM) and an Intermet Systems iMET-XQ2 meteorology sensor (Fig. 5). The copter had a ~15 minute flight time with the on-board sensors without a camera. The POM measures ambient ozone using UV absorption and active humidity subtraction by measuring a whole air sample and an ozone scrubbed sample in a 10-s duty cycle. The POM records data to its internal data storage at 10 s interval with a log number and time stamp along with GPS coordinates and instrumentation metrics (optical cell pressure and temperature). The iMET system records temperature, humidity, and pressure along with GPS coordinates and a time stamp to internal data storage. Each instrument (the POM and iMET) had individual data logging systems and separate power supplies. Both the POM and the iMET had GPS capabilities with the POM logging inconsistently and the iMET logging GPS more consistently. Each instrument and the UAS flight recorder logged time stamps. The iMET recorded observations of temperature, relative humidity, humidity temperature and pressure at a frequency of 10 Hz. The POM recorded ozone observations at a frequency of 0.1 Hz. The POM, iMET and M210 time-stamps drifted up to 60 seconds from the other logged data. The flight log recorded the M210 positioning (altitude,

https://doi.org/10.5194/essd-2021-310
Preprint. Discussion started: 4 November 2021

latitude, longitude) at 100 Hz. The M210 flight logs, iMET data and POM data were each downloaded separately after each series of flights.

Figure 5: DJI M210 multirotor UAS with bracket-mounted POM and iMET

3.3 Chiwaukee Lidar System

A Halo Photonics Stream Line XR Doppler lidar (Pearson et al. 2009) was deployed on the roof of the Chiwaukee Prairie air monitoring station (Fig. 6), approximately 3 m AGL. This is the same system that is regularly deployed as part of the Space Science and Engineering Center (SSEC) Portable Atmospheric Research Center, SPARC, (Wagner et al., 2019). The Doppler lidar actively emits pulses of near-infrared

https://doi.org/10.5194/essd-2021-310
Preprint. Discussion started: 4 November 2021


Open Access Earth System Science Data Discussions

radiation at a wavelength of 1.5 μm. This wavelength is long enough that molecular scattering causes little attenuation of the signal, but it is short enough that it is sensitive to aerosols that are suspended within the planetary boundary layer.

The Doppler lidar uses velocity-azimuth display (VAD) scans of the Doppler lidar to retrieve profiles of wind speed and direction. In VAD, an instrument capable of measuring along-beam velocity (like a Doppler radar or lidar) stares at multiple azimuths at a non-zenith elevation angle over a short period of time, and then reconstructs the profile of winds above the lidar by assessing how the along-beam velocity changes as a function of azimuth and range. For WiscoDISCO-21, the VAD scans were configured with six azimuthal stares per profile (at azimuths of 0 º, 60 º, 120 º, and so on) with an elevation angle of 70 º. Range gates were 18 m. VAD scans were conducted every 4 min and each VAD took approximately 45 s to complete. Between VADs, the lidar reverted to vertical stares in order to capture profiles of backscatter and vertical velocity. Since the lidar depends on the presence of scatterers to have a detectable signal return, the depth of the retrieved wind profiles varied significantly throughout the experiment from as shallow as 200 m to as deep as 2 km.

https://doi.org/10.5194/essd-2021-310
Preprint. Discussion started: 4 November 2021

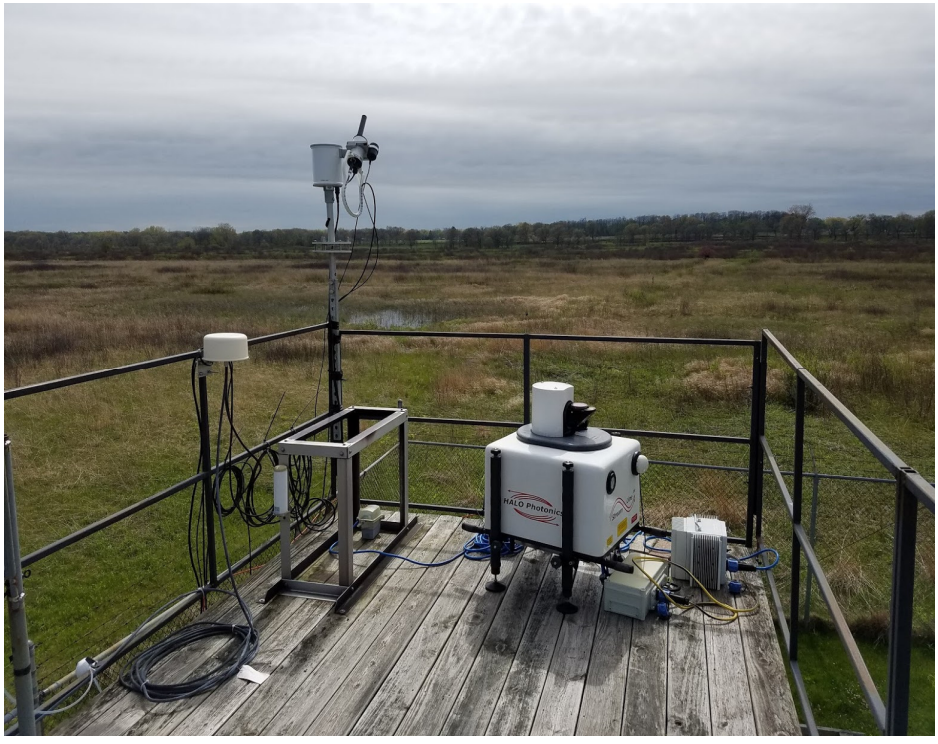

Figure 6: Roof of the Chiwaukee Prairie air monitoring system, showing the PANDORA (upper left) and Doppler lidar (right-center). The wooden floor pictured here is approximately 3 m above ground level.

4. Data processing and quality control

4.1 University of Colorado RAAVEN UAS

Data collected by the different sensors carried by the RAAVEN during WiscoDISCO-21 were logged at a variety of different logging rates. The finewire system was logged at 250 Hz, the fastest rate of all of the sensors. The BST MHP was logged at 100 Hz, the VectorNav VN-300 at 50 Hz, the Melexis IR sensors and variables related to finewire status were logged at 20 Hz, while data collected from the PixHawk autopilot and Vaisala RSS421 sensors were logged at 5 Hz. Each logging event carried out by the FlexLogger includes a sample time from the logger CPU clock, allowing for post-collection time

https://doi.org/10.5194/essd-2021-310
Preprint. Discussion started: 4 November 2021


Open Access Earth System Science Data Discussions

alignment between the different sensors. These sample times, along with artificial 5, 20, 50, 100, and 250 Hz clocks spanning the sample times between initial GPS lock and the last recorded sample time for the VN-300, are used to align the different variables to a set of common clocks, primarily through one-dimensional linear interpolation. One exception to the linear interpolation is the yaw estimate, which is circular in nature (ranging between -180 and 180 degrees), and therefore uses a "nearest" interpolation to ensure that the transition from 360 to 0 degrees is not represented as 180. During this interpolation process, a limited number of points sharing a common sample time with another point are removed from the record. Once these time variables are established, a *base_time* variable is established using the 250 Hz time stamp, and offsets from *base_time* are then calculated for all different logging resolutions.

The resampled (in time) dataset includes a variety of derived and measured quantities. Aircraft position, including latitude, longitude, and altitude, are measured by the VN-300. The aircraft altitude is corrected using a combination of various inputs from onboard GPS and pressure altimeters, as neither of these altitude estimates can be used reliably as a definite flight altitude. Pressure altitude is subject to drift over the duration of a single flight due to atmospheric evolution over a 2.5-hour window, potentially resulting in values at landing that are higher or lower than those at take-off. Similarly, the accuracy of the GPS altitude is insufficient to capture the vertical position of the aircraft to the level of detail required. To calculate a true altitude, a combination of the autopilot altitude, VN-300 altitude, and VN-300 pressure are used. First, a *flight_flag* variable is computed using airspeed and altitude information from the autopilot. Any data points with airspeed exceeding 10 m s^{-1} and an altitude exceeding 5 m AGL is flagged as a time when the aircraft is flying (*flight_flag*=1). The point at 200 samples (4 seconds) prior to the first point in the record where the aircraft is deemed to be flying is recorded as the initial take-off index, while the data point at 200 samples (4 seconds) after the last point in the record where the aircraft is deemed to be flying is recorded as the landing index. The difference between the autopilot altitude at these two indices is added into the flight record on a timestep-by-timestep basis, to correct for temporal drift in pressure. A linear fit is then calculated to relate the VN-300 pressure and the difference between the VN-300 reported altitude and the autopilot reported altitude. This pressure-dependent altitude correction is then applied to the VN-300-reported altitude to derive a final altitude.

https://doi.org/10.5194/essd-2021-310
Preprint. Discussion started: 4 November 2021


Open Access Earth System Science Data Discussions

336

337 Wind estimation from fixed-wing aircraft requires the combination of several different measurements
338 related to airspeed, aircraft motion, and airflow over the aircraft (see van den Kroonenberg et al., 2008).
339 These measurements need to be of sufficient quality, and angular offsets and logging delays need to be
340 considered and removed. For RAAVEN, true airspeed (TAS) biases have a large impact on derivation of
341 wind speed, while the angular offsets between the MHP and INS and time-lag between the GPS and in
342 situ measurements have smaller impacts. These potential sources of error are corrected for using an
343 optimization technique, where small adjustments are made to the individual parameters and the
344 combination that results in the wind solution with the smallest overall variance is selected as the correct
345 winds.

346

347 For the RAAVEN WiscoDISCO-21 dataset, TAS is calculated using measurements from the MHP and
348 RSS421 probe using equation 1 from (Brown et al., 1983):

349 $$TAS_i = \sqrt{\frac{2\bar{q}}{\rho}} \quad (1)$$

350 where ρ is the density of air calculated using the static pressure reported from the MHP, temperature from
351 the RSS421, and the specific gas constant for dry air, $\bar{q}$ is defined as:

352 $$\bar{q} = \frac{p_0}{1-\frac{9}{4}sin^2\,\theta_a} \quad (2)$$

353 where $\sin^2\theta_a$ is the total aerodynamic angle of the MHP, calculated using the angle of attack (α) and
354 sideslip angle (β) reported by the MHP.

355

356 Based on testing in a temperature chamber, the pressure sensors used in this version of the MHP were
357 found to have non-linear temperature dependencies. This requires the application of an additional
358 temperature-dependent correction to ensure that an artificial alteration of TAS with altitude was not
359 present. Additional information on the calculation of airspeed and other quantities from the MHP can be
360 found in (de Boer et al., 2021a).

361

https://doi.org/10.5194/essd-2021-310
Preprint. Discussion started: 4 November 2021

Derivation of the RAAVEN's thermodynamic measurements included multiple processing steps. First, data from the two RSS421 sensors are averaged to attempt to reduce the influence of any solar exposure of the sensors. Previous evaluations of the potential for solar contamination have not revealed any specific biases on the observation (see de Boer et al., 2021a). Over the course of the WiscoDISCO-21 campaign, the two sensors varied by less than 0.5 °C (Fig. 7). The averaged temperature time series was then used to calibrate the coldwire data by applying a linear fit to the relationship between the coldwire voltage and the temperature measured by the RSS421 sensor. The RSS421 relative humidity values were also averaged. Typically, the RH measurements agreed to within 2%.

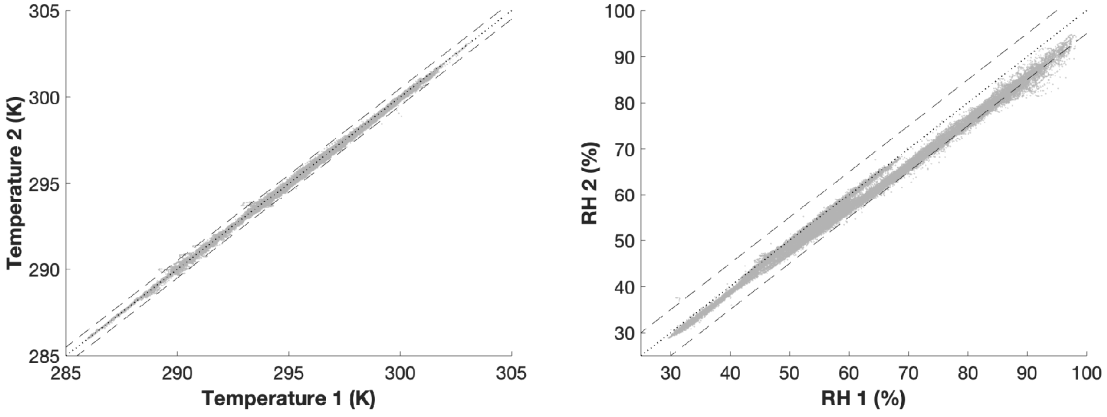

Figure 7: A comparison of temperature (left) and relative humidity (right) observations from the two Vaisala RSS-421 sensors on RAAVEN for all flights. The dotted lines represent a one-to-one agreement, with the dashed lines representing 0.5 degree (for temperature) and 5% (for relative humidity) deviation from perfect agreement.

All quantities measured by the RAAVEN have data quality flags associated with them. For the RSS421-derived temperature, the flag is set to zero for good data, and set to one for times when any of the following occur: a) the absolute value of the difference between the temperature from either individual sensor and the output temperature is greater than 0.5 °C, b) the absolute value of the difference between the output temperature and the temperature from the EE-03 sensor on the MHP exceeds 5 °C, c) the recorded error

https://doi.org/10.5194/essd-2021-310
Preprint. Discussion started: 4 November 2021


Open Access Earth System Science Data Discussions

382 flag of either RSS421 sensor is active, or d) the aircraft is not flying. For the RH measurement from the
383 RSS421, a similar set of criteria are used to activate the data quality flag, except the limits are set to be
384 6% between RSS421 sensors, and 15% between the output RH value and the MHP-provided RH value.
385 The coldwire temperature data quality flag is activated when the difference between the coldwire
386 temperature and either of the RSS421 temperatures exceeds 1 °C, when the absolute value of the
387 difference between the coldwire temperature and the MHP temperature exceeds 3 °C, when the coldwire
388 voltage is observed to fall outside of the 0-4 V analog range, or when the aircraft is not flying. Finally,
389 the pressure quality control flag for the pressure measurement from the VN-300 is activated if the absolute
390 value of the difference between the reported VN-300 static pressure and that measured by either of the
391 RSS421 sensors exceeds 2.5 hPa. The RSS421 pressure measurements are not used because they are
392 believed to be biased low due to the airflow passing over their location on the aircraft.
393
394 In addition to the flags discussed above, we include a 3-stage flag for the wind measurements, which is
395 set to 0 (good data), 1 (suspect data) or 2 (bad data). Data are determined to be bad if any of the following
396 conditions were met:
397 - The measured angle of attack or sideslip exceeds 20 degrees, with values between 10-20
398 degrees are flagged as "suspect"
399 - The true airspeed (TAS) is below 10 m s^{-1}
400 - Any of the MHP ports are deemed to be blocked, as determined by the differential pressure
401 value for any of the sensors falling below -100 Pa
402 - The moving window variance of the MHP-derived TAS over 40 seconds is less than 5
403 - The aircraft is not flying
404 - The difference between the MHP TAS and that from the Pitot probe is greater than 5 m s^{-1}
405
406 Finally, we included two additional flags in the datastream to allow data users to better understand aircraft
407 flight state and support sampling during specific phases of flight. These flags include the "Flight_Flag"
408 introduced previously, as well as a "Flight_State" flag. The "Flight_State" flag includes information on
409 whether the is flying straight (0) or is turning (1) in the ones place, whether the aircraft is descending (0),

https://doi.org/10.5194/essd-2021-310
Preprint. Discussion started: 4 November 2021


Open Access Earth System Science Data Discussions

level (1), or ascending (2) in the tens place, and whether the aircraft is in flight (1) or not (0) in the hundreds place. If, for example, a data user wanted to analyze straight, level flight legs, they would search for data with "Flight_State" equal to 110. These flags are derived from information from a combination of sensors, including the altitude variable described above, the aircraft yaw, and the "Flight_Flag" variable described earlier on in this paragraph.

The accuracy of the RAAVEN observations has been evaluated in previous studies. For example, a comparison of RAAVEN data with measurements collected by radiosondes launched from the Barbados Cloud Observatory was conducted in recent work from de Boer et al., (2021b). While radiosondes in that evaluation were launched approximately 20 km to the southeast, the air sampled by both systems was largely representative of the marine boundary layer, implying limited spatial variability. In that evaluation, the observations from the RAAVEN were very well correlated with those from the radiosondes and do not show any positive or negative bias, supporting the idea that the RAAVEN measurements provide an accurate depiction of the lower atmosphere. In addition, recent work allowed for direct comparison of RAAVEN data to observations collected by radiosondes and a 60 m tower at the US Department of Energy's Southern Great Plains (SGP) research site. That study, de Boer et al. (2021a), similarly provided confidence in the RAAVEN observations, showing close statistical agreement between the different data sources.

4.2 M210 UAS

Data from the M210 flight controller, the POM and the iMET were all logged to individual instrument internal data storage with independent timestamps. The average flight time of the M210 was 13.96 min. The POM instrument logged data every 10 s. The iMET logged data every 0.1 s and the M210 flight log recorded UAS GPS positioning and flight statistics at 0.01 s intervals. The ozone concentrations from the POM are adjusted to calibrated values, where ozone calibrations were conducted before every set of 2 flights for the M210 using a 2BTech Model 306 ozone calibration source (Fig. 8). Data quality flags are established as 0 = no concern, 1 = time flag, 2 = calibration and time flag. The time flag indicates flights where the time offset between the M210 and the instrument time offset is large (iMET > 10 s or

https://doi.org/10.5194/essd-2021-310
Preprint. Discussion started: 4 November 2021


Open Access Earth System Science Data Discussions

438 POM > 30 s). The calibration flag indicates when the POM was not responsive to the ozone calibration
439 source (Flight 5 on May 24) after an over-water flight. All times were averaged to 90 seconds and
440 compressed to the time window of observations for a single M210 ascent using the M210 timestamp. A
441 time stamp for 90s averaged data from all instrumentation on the M210 was generated by using the M210
442 timestamp as primary and adjusting to a time offset in either the POM or the iMET for the start of a flight,
443 then averaged each variable for every 90 second interval of the flight. A 1σ standard deviation is
444 presented as the uncertainty for the 90-s averages. The iMET observations of temperature, relative
445 humidity, pressure and humidity temperature are presented using the 90-s averages with uncertainty as
446 1σ standard deviations. Each flight ascent start and end were determined by observed changes in
447 atmospheric pressure by the iMET sensor, altitude change in the M210, or noted time of ascent in field
448 notebook for the POM. The altitudes for each observation were obtained by averaging the M210 flight
449 log altitude data for the 90-s timestamps. The flight data timestamps varied slightly for each data source.
450 The POM time drift was the most pronounced, with an average difference between the iMet of ~ 24 s.
451 The POM's time was adjusted manually throughout the campaign as the time would drift over the course
452 of one flight. The average difference between the iMet and the M210 over 20 flights was ~ 4 s. Only
453 20% of flights had a time-difference between iMET and M210 greater than 10 seconds. Instrument battery
454 loss occurred for the iMET system which resulted in lost data for a few flights on May 26, 2021.

https://doi.org/10.5194/essd-2021-310
Preprint. Discussion started: 4 November 2021

Open Access Earth System Science Data Discussions

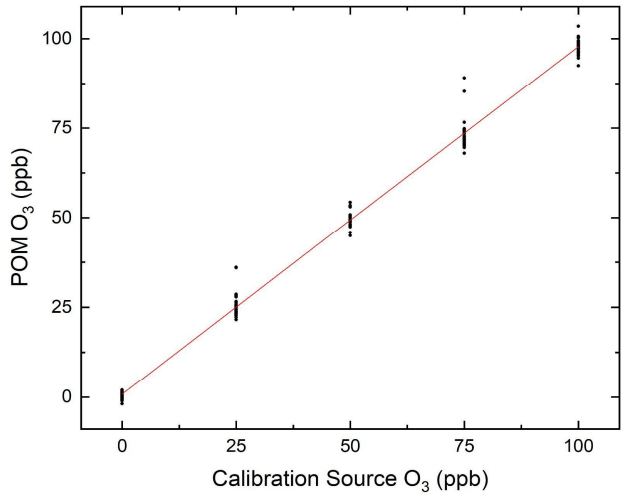

Figure 8: A sample POM calibration from May 24, 2021. The linear regression fit gives: $y = 0.9689$ (± 0.0061) $x + 0.83$ (±0.35), $R^2 = 0.9937$. Each calibration concentration had a 5-minute duration with the POM logging 10-s data.

Intercomparison between observations made via instrumentation on the M210 at 5 m AGL and at the Wi-DNR ground station show a linear agreement between the observations (Fig. 9). The linear agreement is better for the iMET temperature and the ground station temperature with $R^2 = 0.970$ in comparison to $R^2 = 0.955$ for O_3 observations. The O_3 linear fit, $O_{3\,(POM)} = 0.944$ (± 0.044) $O_{3\,(DNR)}$ - 3.3 (±1.9), has a negative intercept. The uncertainties in the POM's O_3 concentrations are much larger than uncertainties in the ground station instrumentation. The linear agreement between the different instrumentation on separate observation platforms demonstrates that the M210 platform instrumentation provides an accurate, albeit less precise representation of the atmosphere.

https://doi.org/10.5194/essd-2021-310
Preprint. Discussion started: 4 November 2021

469

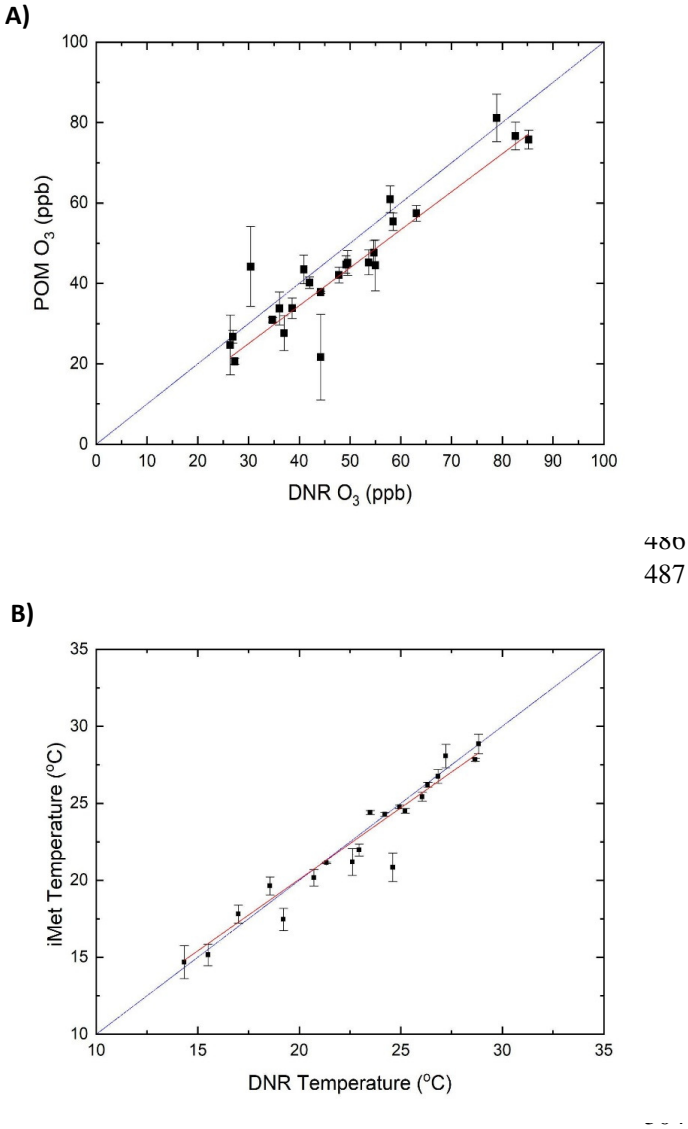

486
487

505 **Figure 9**: Intercomparsion between measurements from instrumentation on the M210 at 5 m AGL and
506 at the WI-DNR ground station for a) O_3 (ppb) observations and b) temperature (° C). Blue lines depict
507 1:1 agreement and red lines depict the linear regression best fit with a) $O_{3\,(POM)} = 0.944\ (\pm 0.044)\ O_{3\,(DNR)} - 3.3\ (\pm 1.9)$, $R^2 = 0.955$, and b) $T_{iMET} = 0.929(\pm 0.038)\ T_{DNR} + 1.48(\pm 0.93)$, $R^2 = 0.970$.
508
509

https://doi.org/10.5194/essd-2021-310
Preprint. Discussion started: 4 November 2021


Open Access Earth System Science Data Discussions

5. Data Availability and File Structure

A community data repository has been established for this field campaign at https://zenodo.org/communities/wiscodisco21/. The data sets in the repository cover the merged iMET and POM data sets from the M210 (DOI:10.5281/zenodo.5160346) as .txt files, the RAAVEN dataset (DOI: 10.5281/zenodo.5142491) as .cdf files, and the doppler lidar wind profiler (DOI: 10.5281/zenodo.5213039) as .cdf files. M210 files have a naming convention that includes WiscoDisco_M210_YYYYMMDD_F#, where the flight number for the day is indicated by F#. RAAVEN files have a naming convention that includes WiscoDisco_CU-RAAVEN_YYYYMMDD_hhmmss_B1.nc, where YYYYMMDD is the year, month and day that the data were collected, hhmmss is the time of power on for the aircraft, and B1 is the data processing level, where B1 files have had data quality checks and post-processing (e.g. coldwire calibration and wind estimation) applied. The Doppler lidar files have a naming convention that includes chiwaukee_wind_profiles_YYYYMMDD and chiwaukee_stare_YYYYMMDD. All datasets include geospatial information (latitude, longitude, altitude) and timestamps in UTC.

6. Summary

The 2021 WiscoDISCO field campaign incorporated the use of two UAS platforms for meteorological and chemical measurements in the atmosphere, a multirotor completing vertical profiles up to 120 m AGL and a fixed wing executing flight patterns up to 500 m AGL alongside a Lidar WindPro instrument capable of sensing winds and aerosol backscatter from altitudes of 100-2000 m AGL. The overlapping domains are useful for characterizing low altitude mesoscale meteorology of the lake breeze at a shoreline environment that regularly observes ozone enhancement events during onshore flow. Data from all instruments and platforms have been compiled, quality-control tested and uploaded to a community repository. The collaborative field campaign involved teams from 4 different universities and obtained continuous lidar data in conjunction with 24 flight hours of fixed wing and 6 flight hours of multi-rotor vertical profiles on days likely impacted by lake breeze.

https://doi.org/10.5194/essd-2021-310
Preprint. Discussion started: 4 November 2021

Open Access Earth System Science Data Discussions

538 The WiscoDISCO-21 project demonstrates how UAS can be used to sample a complex circulation
539 near to the surface without causing major disruption to people, wildlife and ecosystems in the area. An
540 example of a characterization of lake breeze incursion is shown in Figures 10 and 11, which include the
541 temperature profiles from the M210 and RAAVEN (Fig. 10) and Doppler lidar u wind component (Fig.
542 11). The temperature profiles from the M210 and RAAVEN show a notable temperature inversion in the
543 late afternoon below 150 m and the Doppler lidar u wind component shows easterly winds arriving after
544 18:00 UTC. The combination of u component winds from Doppler lidar and the temperature observations
545 from the UAS platforms are consistent in demonstrating a marine layer incursion with maximum height
546 of approximately 250 m AGL at 21:00 UCT collapsing to a height of 100 m AGL by 22:00 UTC. The
547 nonuniform start to the lake breeze onset fluctuated, shown as shifting u component winds from easterly
548 to westerly after 18:00 UTC (Fig 11) and disagreement with the lowest altitude observations from the
549 M210 and RAAVEN between 18:30-19:00 UTC (Fig 10). The distance between the M210 launch site
550 and the RAAVEN landing site complicates the low altitude observations of temperatures between 18:00
551 and 19:00 UTC, which also may indicate the very limited incursion of the lake breeze at that time.

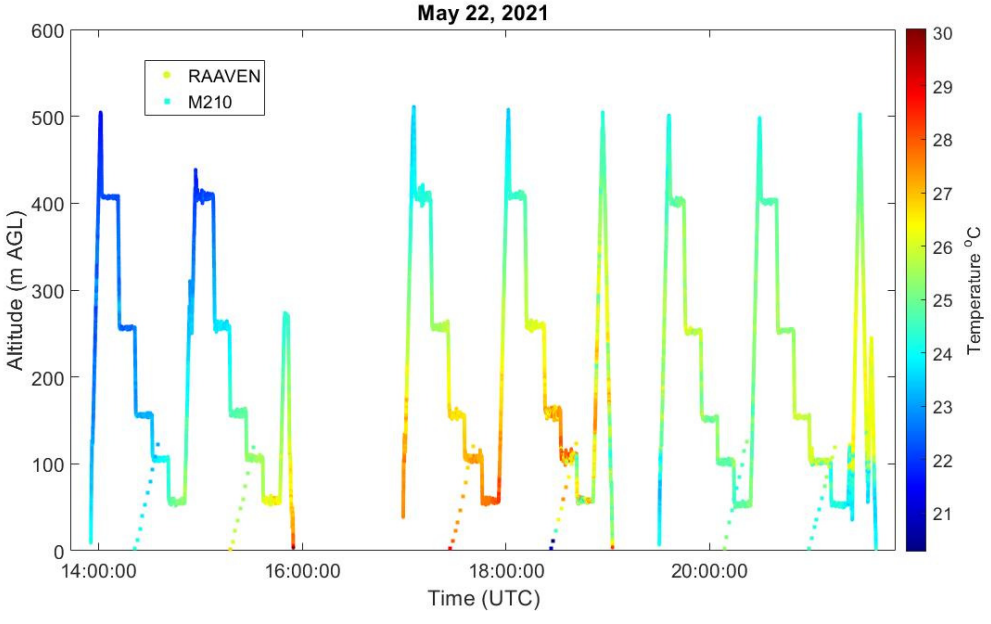

552

https://doi.org/10.5194/essd-2021-310
Preprint. Discussion started: 4 November 2021

553

554 **Figure 10**: Temperatures (° C) measured from University of Colorado RAAVEN (○) and the M120 (□)
555 on May 22, 2021. RAAVEN was flying over-prairie circular spirals Pattern A.

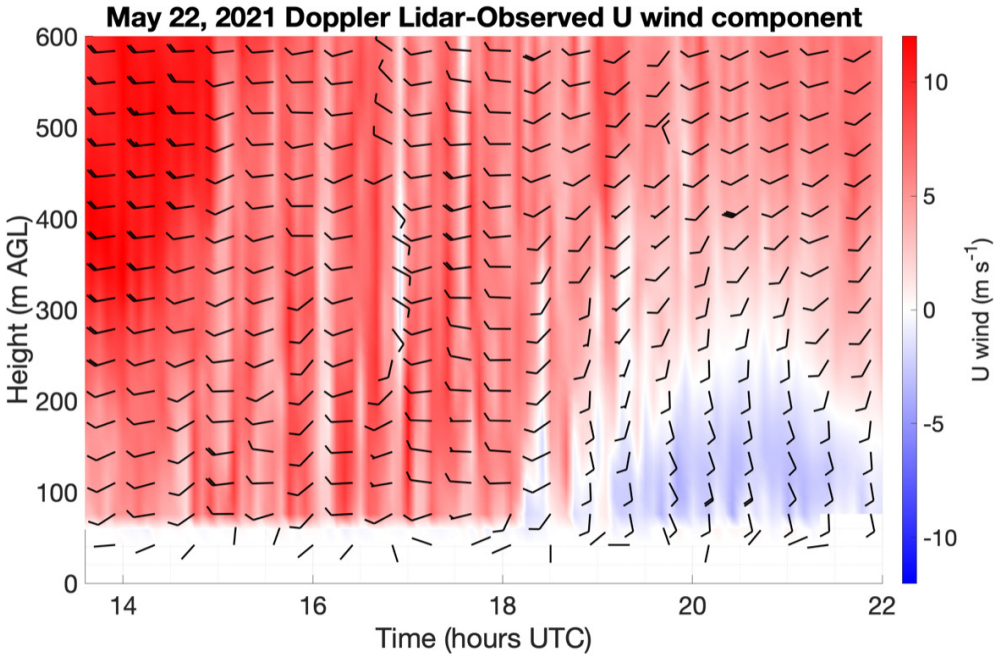

556

557 **Figure 11**: Time/height cross section of the u (zonal) component of the Doppler lidar-observed
558 horizontal winds (in m/s), overlaid with horizontal wind barbs (in kts) plotted according to the standard
559 convention from May 22, 2021. Wind barbs are thinned by a factor of five in the time dimension and a
560 factor of two in the height dimension to aid readability.

561

562 The data from the WiscoDISCO-21 campaign can be used to evaluate the markers for lake breeze
563 incursion overland in winds, temperatures, chemical composition and optical properties (backscatter).
564 The thermodynamic conditions for lake breeze incursion at a local scale can be determined through the
565 evaluation of horizontal and vertical winds, atmospheric stability and potential temperature. The
566 positioning of pollutants with respect to the marine layer markers can also be investigated.

567

568 **Author Contributions.**

https://doi.org/10.5194/essd-2021-310
Preprint. Discussion started: 4 November 2021


Open Access Earth System Science Data Discussions

Patricia A. Cleary is the PI of this project and was responsible for data collection, overseeing data analysis from the M210, field campaign planning and logistics, and the writing and editing of this document. Ben Kies was responsible for data collection for the M210 in the field, Joe Tirado was responsible for data analysis, quality control and data formatting for the repository for the M210, Aidan Voon was responsible for data analysis for the M210. Joe Hupy was responsible for piloting the M210 and the writing and editing of this paper. Gijs de Boer was responsible for coordination and execution of the University of Colorado RAAVEN flights, and for development, writing and editing of the publication. Steve Borenstein and Jonathan Hamilton contributed to the collection of the RAAVEN dataset as field operators, and supported the development of this manuscript. Dale Lawrence supplied instrumentation for the RAAVEN UAS and contributed to the writing of the manuscript. Tim Wagner and R Bradley Pierce were responsible for data collection, data analysis of the doppler lidar instrumentation, and writing and editing this document and R Bradley Pierce assisted in field planning.

Competing Interests.

GB works as a consultant for Black Swift Technologies, who manufacture the multi-hole pressure probe used in the collection of the RAAVEN dataset.

Acknowledgements.

This material is based upon work funded by the National Science Foundation award #1918850. The UW-Eau Claire team acknowledges support from the Student Blugold Commitment Differential Tuition program. The University of Colorado team acknowledges financial support from the University of Wisconsin Eau-Claire through a sub-contract supported by the US National Science Foundation, as well as support from the NOAA Physical Sciences Laboratory. Any opinions, findings, and conclusions or recommendations expressed in this material are those of the author(s) and do not necessarily reflect the views of the National Science Foundation.

https://doi.org/10.5194/essd-2021-310
Preprint. Discussion started: 4 November 2021

600 **References**
601
602
603 Brown, E. N., Friehe, C. A., and Lenschow, D. H.: THE USE OF PRESSURE-FLUCTUATIONS ON
604 THE NOSE OF AN AIRCRAFT FOR MEASURING AIR MOTION, Journal of Climate and
605 Applied Meteorology, 22, 171-180, 10.1175/1520-0450(1983)022<0171:Tuopfo>2.0.Co;2, 1983.
606 Cleary, P. A., Fuhrman, N., Schulz, L., Schafer, J., Fillingham, J., Bootsma, H., McQueen, J., Tang, Y.,
607 Langel, T., McKeen, S., Williams, E. J., and Brown, S. S.: Ozone distributions over southern Lake
608 Michigan: comparisons between ferry-based observations, shoreline-based DOAS observations and
609 model forecasts, Atmospheric Chemistry and Physics, 15, 5109-5122, 10.5194/acp-15-5109-2015,
610 2015.
611 de Boer, G., Borenstein, S., Hamilton, J., Osborn, J., Lawrence, D., Argrow, B., and Intrieri, J.:
612 Measurements from the University of Colorado RAAVEN Uncrewed Aircraft System during
613 ATOMIC, Earth System Science Data, submitted, 2021a.
614 de Boer, G., Elston, J., Houston, A., Pillar-Little, E., Argrow, B., Bell, T., Chilson, P., Choate, C.,
615 Greene, B., Islam, A., Detweiler, C., Jacob, J., Natalie, V., Rhodes, M., Rico, D., Stachura, M.,
616 Lappin, F., Whyte, S., and Wilson, M.: Evaluation and Intercomparison of Small Uncrewed Aircraft
617 Systems Used for Atmospheric Research, in preparation, Journal of Atmospheric and Oceanic
618 Technology, 2021b.
619 Doak, A. G., Christiansen, M. B., Alwe, H. D., Bertram, T. H., Carmichael, G., Cleary, P., Czarnetzki,
620 A. C., Dickens, A. F., Janssen, M., Kenski, D., Millet, D. B., Novak, G. A., Pierce, B. R., Stone, E.
621 A., Long, R. W., Vermeuel, M. P., Wagner, T. J., Valin, L., and Stanier, C. O.: Characterization of
622 ground-based atmospheric pollution and meteorology sampling stations during the Lake Michigan
623 Ozone Study 2017, Journal of the Air & Waste Management Association, 71, 866-889,
624 10.1080/10962247.2021.1900000, 2021.
625 Dye, T. S., Roberts, P. T., and Korc, M. E.: Observations of transport processes for ozone and ozone
626 precursors during the 1991 Lake Michigan Ozone Study, Journal of Applied Meteorology, 34, 1877-
627 1889, 10.1175/1520-0450(1995)034<1877:ootpfo>2.0.co;2, 1995.
628 Elston, J., Argrow, B., Stachura, M., Weibel, D., Lawrence, D., and Pope, D.: Overview of Small Fixed-
629 Wing Unmanned Aircraft for Meteorological Sampling, Journal of Atmospheric and Oceanic
630 Technology, 32, 97-115, 10.1175/jtech-d-13-00236.1, 2015.
631 Foley, T., Betterton, E. A., Jacko, P. E. R., and Hillery, J.: Lake Michigan air quality: The 1994-2003
632 LADCO Aircraft Project (LAP), Atmospheric Environment, 45, 3192-3202,
633 10.1016/j.atmosenv.2011.02.033, 2011.
634 Frew, E. W., Argrow, B., Borenstein, S., Swenson, S., Hirst, C. A., Havenga, H., and Houston, A.: Field
635 observation of tornadic supercells by multiple autonomous fixed-wing unmanned aircraft, Journal of
636 Field Robotics, 37, 1077-1093, 10.1002/rob.21947, 2020.
637 Gronoff, G., Robinson, J., Berkoff, T., Swap, R., Farris, B., Schroeder, J., Halliday, H. S., Knepp, T.,
638 Spinei, E., Carrion, W., Adcock, E. E., Johns, Z., Allen, D., and Pippin, M.: A method for

https://doi.org/10.5194/essd-2021-310
Preprint. Discussion started: 4 November 2021

quantifying near range point source induced O-3 titration events using Co-located Lidar and Pandora measurements, Atmospheric Environment, 204, 43-52, 10.1016/j.atmosenv.2019.01.052, 2019.

Guimaras, P., Ye, J. H., Batista, C., Barbosa, R., Ribeiro, I., Medeiros, A., Zhao, T. N., Hwang, W. C., Hung, H. M., Souza, R., and Martin, S. T.: Vertical Profiles of Atmospheric Species Concentrations and Nighttime Boundary Layer Structure in the Dry Season over an Urban Environment in Central Amazon Collected by an Unmanned Aerial Vehicle, Atmosphere, 11, 10.3390/atmos11121371, 2020.

Hayden, K. L., Sills, D. M. L., Brook, J. R., Li, S. M., Makar, P. A., Markovic, M. Z., Liu, P., Anlauf, K. G., O'Brien, J. M., Li, Q., and McLaren, R.: Aircraft study of the impact of lake-breeze circulations on trace gases and particles during BAQS-Met 2007, Atmospheric Chemistry and Physics, 11, 10173-10192, 10.5194/acp-11-10173-2011, 2011.

Horel, J., Crosman, E., Jacques, A., Blaylock, B., Arens, S., Long, A., Sohl, J., and Martin, R.: Summer ozone concentrations in the vicinity of the Great Salt Lake, Atmospheric Science Letters, 17, 480-486, 10.1002/asl.680, 2016.

Keen, C. S. and Lyons, W. A.: Lake/Land Breeze circulations on the western shore of Lake Michigan, Journal of Applied Meteorology, 17, 1843-1855, 10.1175/1520-0450(1978)017<1843:lbcotw>2.0.co;2, 1978.

Lennartson, G. J. and Schwartz, M. D.: The lake breeze-ground-level ozone connection in eastern Wisconsin: A climatological perspective, International Journal of Climatology, 22, 1347-1364, 10.1002/joc.802, 2002.

Levy, I., Makar, P. A., Sills, D., Zhang, J., Hayden, K. L., Mihele, C., Narayan, J., Moran, M. D., Sjostedt, S., and Brook, J.: Unraveling the complex local-scale flows influencing ozone patterns in the southern Great Lakes of North America, Atmospheric Chemistry and Physics, 10, 10895-10915, 10.5194/acp-10-10895-2010, 2010.

Lyons, W. A. and Cole, H. S.: Photochemical oxidant transport - Mesoscale lake breeze and synoptic-scale aspects, Journal of Applied Meteorology, 15, 733-743, 10.1175/1520-0450(1976)015<0733:potmlb>2.0.co;2, 1976.

Lyons, W. A. and Olsson, L. E.: Detailed mesometeorological studies of air pollution dispersion in Chicago lake breeze, Monthly Weather Review, 101, 387-403, 10.1175/1520-0493(1973)101<0387:dmsoap>2.3.co;2, 1973.

Sills, D. M. L., Brook, J. R., Levy, I., Makar, P. A., Zhang, J., and Taylor, P. A.: Lake breezes in the southern Great Lakes region and their influence during BAQS-Met 2007, Atmospheric Chemistry and Physics, 11, 7955-7973, 10.5194/acp-11-7955-2011, 2011.

Stanier, C. O., Pierce, R. B., Abdi-Oskouei, M., Adelman, Z. E., Al-Saadi, J., Alwe, H. D., Bertram, T. H., Carmichael, G. R., Christiansen, M. B., Cleary, P. A., Czarnetzki, A. C., Dickens, A. F., Fuoco, M. A., Hughes, D. D., Hupy, J. P., Janz, S. J., Judd, L. M., Kenski, D., Kowalewski, M. G., Long, R. W., Millet, D. B., Novak, G., Roozitalab, B., Shaw, S. L., Stone, E. A., Szykman, J., Valin, L., Vermeuel, M., Wagner, T. J., and Whitehill, A. R.: Overview of the Lake Michigan Ozone Study 2017, Bulletin of the American Meteorological Society, doi.org/10.1175/BAMS-D-20-0061.1, 2021.

Vermeuel, M. P., Novak, G. A., Alwe, H. D., Hughes, D. D., Kaleel, R., Dickens, A. F., Kenski, D., Czarnetzki, A. C., Stone, E. A., Stanier, C. O., Pierce, R. B., Millet, D. B., and Bertram, T. H.:

https://doi.org/10.5194/essd-2021-310
Preprint. Discussion started: 4 November 2021

680 Sensitivity of Ozone Production to NOx and VOC Along the Lake Michigan Coastline, Journal of
681 Geophysical Research-Atmospheres, 124, 10989-11006, 10.1029/2019jd030842, 2019.
682 Wagner, T. J., Klein, P. M., and Turner, D. D.: A NEW GENERATION OF GROUND-BASED
683 MOBILE PLATFORMS FOR ACTIVE AND PASSIVE PROFILING OF THE BOUNDARY
684 LAYER, Bulletin of the American Meteorological Society, 100, 137-153, 10.1175/bams-d-17-
685 0165.1, 2019.
686 Wagner, T. J., Czarnetzki, A. C., Christiansen, M., Pierce, R. B., Stanier, C. O., Dickens, A. F., and
687 Eloranta, E. W.: Observations of the Development and Vertical Structure of the Lake Breeze
688 Circulation During the 2017 Lake Michigan Ozone Study, Submitted, 2021.
689 Wentworth, G. R., Murphy, J. G., and Sills, D. M. L.: Impact of lake breezes on ozone and nitrogen
690 oxides in the Greater Toronto Area, Atmospheric Environment, 109, 52-60,
691 10.1016/j.atmosenv.2015.03.002, 2015.
692 Wildmann, N., Ravi, S., and Bange, J.: Towards higher accuracy and better frequency response with
693 standard multi-hole probes in turbulence measurement with remotely piloted aircraft (RPA),
694 Atmospheric Measurement Techniques, 7, 1027-1041, 10.5194/amt-7-1027-2014, 2014.
695